AIAA JOURNAL
Vol. 34, No. 5, May 1996

Self-Similar Viscous Incompressible Flow Along an Unbounded Corner

V. I. Vasiliev*
Central Institute of Aviation Motors, Moscow 111250, Russia

The self-similar viscous flow of incompressible fluid along the right-angle unbounded corner with nonzero streamwise pressure gradient is considered. The corner layer equations for this case are derived, and their asymptotic series are analyzed. It is shown that self-similar corner layer equations have two solutions, even at a zero streamwise pressure gradient. The numerical procedure for the integration of corner layer equations is developed, and numerical calculations are performed at several values of power exponent for a streamwise pressure gradient distribution.

Nomenclature

m	= power exponent
P	= cross plane averaged pressure
p	= pressure variations in cross planes
U, V, W	= velocity components
u, v, w	= normalized velocity components
x, y, z	= Cartesian coordinates
ζ, η	= similarity coordinates
θ	= modified streamwise vorticity
ν	= kinematic viscosity
ρ	= density
ϕ, ψ	= transformed cross velocities
Ω, ω	= streamwise vorticity

Introduction

SELF-SIMILAR viscous flow along an unbounded corner without a pressure gradient was analytically and numerically studied by several authors.[1-5] According to Rubin[1] it was Pearson who first (in 1957) obtained the numerical solution of corner layer self-similar equations. Pearson, however, did not take into account the algebraic decay of secondary flows. The improved asymptotic expansions of corner layer equations were obtained by Rubin[1] and Pal and Rubin.[2] Rubin and Grossman[3] performed the numerical calculations using these asymptotic expansions as boundary values. They had to solve the corner layer equations iteratively and minimize the error in the continuity equations to find the unknown constant in the second-order terms. Recently, the self-similar corner layer equations were numerically solved by Ghia[4] and Michail and Ghia,[5] who also extended the calculations to the compressible case with heat transfer. Ghia did not use the asymptotic expansions, because the boundary conditions were imposed at infinity and the infinite flow region was transformed into a finite computational domain. In all of the mentioned works, flow without a streamwise pressure gradient was considered.

In present work, the corner flow with a nonzero streamwise pressure gradient was studied. The corner layer equations for this case were derived, and their asymptotic series was analyzed. It was shown that self-similar corner layer equations have two solutions, even at zero streamwise pressure gradient. The numerical procedure for integration of the corner layer equations was developed, and numerical calculations were performed at several values of power exponent for a streamwise pressure gradient distribution.

The results of this work can be used for qualitative analysis of a corner flow and as a base for corner flow stability study. They may be also useful for testing of Navier–Stokes solvers.

Received Nov. 26, 1994; revision received June 30, 1995; accepted for publication July 14, 1995.

*Head of Group, Gas Dynamic Department, 111250, Aviamotornaya St., 2.

Mathematical Model

The scheme of the flow and the coordinate system are presented in Fig. 1a. Assuming a homogeneous streamwise pressure gradient across the flow (i.e., dP/dx is a function of x only) one can describe the flow using parabolic equations.[6] The streamwise pressure gradient is connected to the streamwise velocity outside the boundary layer by the relationship

$$\frac{1}{\rho}\frac{dP}{dx} = -U_e\frac{dU_e}{dx}, \qquad U_e(x) = \lim_{\sqrt{y^2+z^2}\to\infty} U(x, y, z)$$

Assuming the power law for external velocity ($U_e = Cx^m$) one can obtain the self-similar solution. The similarity variables are the Falkner–Skan variables[7]

$$\eta = y/\delta(x), \qquad \zeta = z/\delta(x)$$

where

$$\delta(x) = \sqrt{\frac{2\nu}{(m+1)C}}\,x^{(1-m)/2}$$

$$u = U/U_e,\ v = V/V_0,\ w = W/V_0,\ \pi = p/\rho V_0^2$$

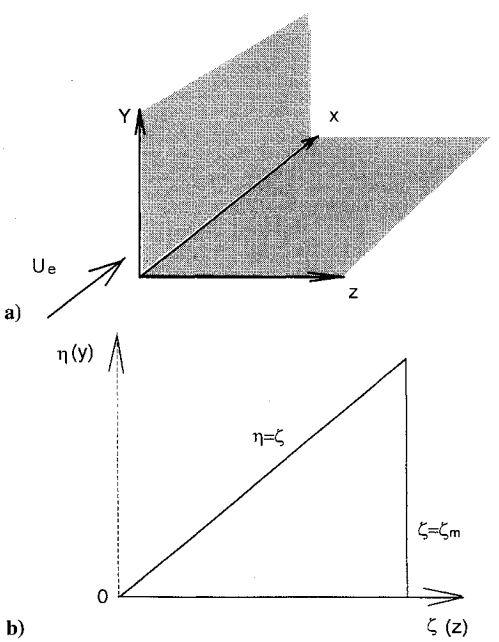

Fig. 1 Scheme of flow.

where

$$V_0 = \sqrt{\frac{C\nu}{(m+1)2}}\,x^{(m-1)/2}$$

Instead of primitive variables v, w, and π it is more convenient to introduce the transformed variables defined as

$$\varphi = \frac{(1-m)\eta u - v}{m+1}, \qquad \psi = \frac{(1-m)\zeta u - w}{m+1}, \qquad \theta = \psi_\eta - \varphi_\zeta$$

where the subscripts indicate derivatives with respect to the corresponding coordinates.

The self-similar corner layer equations in these variables are written as

$$\begin{aligned} &\Delta u + \varphi u_\eta + \psi u_\zeta + [2m/(m+1)](1-u^2) = 0 \\ &\Delta\theta + \varphi\theta_\eta + \psi\theta_\zeta + [2u\theta/(m+1)] \\ &\quad + 2[(m-1)/(m+1)]u(\zeta u_\eta - \eta u_\zeta) = 0 \\ &\varphi_\eta + \psi_\zeta = 2u/(m+1) \qquad \psi_\eta - \varphi_\zeta = \theta \end{aligned} \tag{1}$$

where

$$\Delta = \frac{\partial^2}{\partial\eta^2} + \frac{\partial^2}{\partial\zeta^2}$$

For $m = 0$ (i.e., at zero streamwise pressure gradient) these equations are the same as considered in Refs. 1–3.

Equations (1) were solved numerically. The computational domain is shown in Fig. 1b as a solid line. Because of symmetry, only the region below the diagonal may be considered. In this case the no-slip conditions are prescribed on the wall, the symmetry conditions on the diagonal, and the asymptotic conditions at the right boundary of the calculation domain. The latter can be obtained by asymptotic expansion of Eqs. (1) at $\zeta \to \infty$.

Following Pal and Rubin[2] we found the asymptotic solution in the form

$$\begin{aligned} u &= u_0(\eta) + u_1(\eta)/\zeta + \mathcal{O}(1/\zeta^2) \\ \varphi &= \varphi_0(\eta) + \varphi_1(\eta)/\zeta + \mathcal{O}(1/\zeta^2) \qquad \text{at} \quad \zeta \to \infty \\ \psi &= \psi_0(\eta)\zeta + \psi_1(\eta) + \psi_2(\eta)/\zeta + \mathcal{O}(1/\zeta^2) \\ \theta &= \theta_0(\eta)\zeta + \theta_1(\eta) + \theta_2(\eta)/\zeta + \mathcal{O}(1/\zeta^2) \end{aligned} \tag{2}$$

The numerical calculations of high-order terms is a rather elaborate process that needs rather lengthy computer codes and additional computer time. Moreover, according to Pal and Rubin,[2] the second-order terms are defined up to an unknown constant. Because of these circumstances only the two main terms (zero order for ψ and θ and first order for u and φ) were considered here. The residual connected with boundary conditions, however, was minimized by the appropriate location of the right computational boundary (the influence of boundary location is discussed subsequently).

Inserting Eqs. (2) into Eqs. (1) and combining the coefficients at the same powers of ζ one can obtain the sets of ordinary differential equations. The equations for the leading terms are written as follows:

$$\begin{aligned} &u_0'' + \varphi_0 u_0' + [2m/(m+1)]\left(1-u_0^2\right) = 0 \\ &\theta_0'' + \varphi_0\theta_0' + \psi_0\theta_0 + [2/(m+1)]u_0\theta_0 \\ &\quad + 2[(m-1)/(m+1)]u_0u_0' = 0 \\ &\varphi_0' + \psi_0 = [2/(m+1)]u_0; \qquad \psi_0' = \theta_0 \end{aligned} \tag{3}$$

where primes denote differentiation with respect to η.

For the next term the corresponding relationships are

$$\begin{aligned} &u_1'' + (\varphi_1 u_0' + \varphi_0 u_1') - \psi_0 u_1 - [4m/(m+1)]u_0u_1 = 0 \\ &\theta_1'' + (\varphi_1\theta_0' + \varphi_0\theta_1') + \psi_1\theta_0 + [2/(m+1)](u_1\theta_0 + u_0\theta_1) \\ &\quad + 2[(m-1)/(m+1)](u_1u_0' + u_1'u_0) = 0 \\ &\varphi_1' = [2/(m+1)]u_1; \qquad \psi_1' = \theta_1 \end{aligned} \tag{4}$$

Each set of equations must be accompanied by six boundary conditions. For Eqs. (3) they have the form

$$\begin{aligned} &\eta = 0: u_0 = \varphi_0 = \psi_0 = 0; \qquad \eta \to \infty: u_0 \to 1 \\ &\theta_0 \to 0, \qquad \psi_0 \to 1/(m+1) \end{aligned}$$

Conditions at $\eta = 0$ are no-slip conditions. Far from the wall ($\eta \to \infty$) the solution must be matched with irrotational external flow with equal cross velocities on a diagonal. The latter requirement defines the value of $\psi_0(\infty)$. [Actually, at $\eta \to \infty$ v_0 tends to $-m\eta$, thus, in order to obtain equal cross velocities on the diagonal it needs to assume $w_0 \to -m\zeta$ and, hence, $\psi_0 \to 1/(m+1)$.]

Taking into account that $\psi_0' = \theta_0$, one can reduce the boundary value problem for leading term to

$$\begin{aligned} &u_0'' + \varphi_0 u_0' + [2m/(m+1)]\left(1-u_0^2\right) = 0 \\ &\psi_0'' + \varphi_0\psi_0' + \psi_0^2 - [1/(m+1)^2] \\ &\quad + [(1-m)/(1+m)]\left(1-u_0^2\right) = 0 \\ &\varphi_0' + \psi_0 = [2/(m+1)]u_0 \\ &u_0(0) = \varphi_0(0) = \psi_0(0) = 0 \\ &u_0(\infty) = 1, \qquad \psi_0(\infty) = [1/(m+1)] \end{aligned} \tag{5}$$

Solving the problem (5) one can find $\lambda = \lim_{\eta\to\infty}[\varphi_0 - \eta/(m+1)]$ and then obtain the boundary conditions for system (4), which are written as follows:

$$\begin{aligned} &\eta = 0: u_1 = \varphi_1 = \psi_1 = 0 \\ &\eta \to \infty: u_1 \to 0, \quad \theta_1 \to 0, \quad \psi_1 \to \lambda \end{aligned}$$

The equations for u_1 and φ_1 uncouple, and the single solution of these equations are $u_1 = \varphi_1 \equiv 0$. Thus, the boundary value problem for the second term is reduced to

$$\begin{aligned} &\psi_1'' + \varphi_0\psi_1' + \psi_0\psi_1 - [\lambda/(m+1)] = 0 \\ &\psi_1(0) = 0; \qquad \psi_1(\infty) = \lambda; \qquad \theta_1 = \psi_1' \end{aligned} \tag{6}$$

This problem as well as all other problems for higher order terms, is linear and has a unique solution. On the other hand, the problem for the leading term is nonlinear. It should be noted also that this nonlinear problem does not coincide with the Falkner–Skan problem due to the presence of cross velocity w in the continuity equation.

It is known that the Falkner–Skan problem has two solutions at negative m. This statement may be proved by asymptotic analysis of the Falkner–Skan equation. Using the preceding notations the Falkner–Skan equation may be written as

$$u_0'' + \varphi_0 u_0' + \beta\left(1-u_0^2\right) = 0; \qquad \varphi_0' = u_0; \qquad \beta = [2m/(m+1)]$$

At $\eta \to \infty$ the solution of this equation may be obtained in form $u_0 = 1 + u$ and $\varphi_0 = \eta + \lambda + \varphi$, where u and φ are small disturbances. Using linear theory one can reduce the Falkner–Skan equation to

$$u'' + (\eta + \lambda)u' - 2\beta u = 0$$

According to the Liouville–Green approximation[8] the asymptotic solution of this linear equation is follows:

$$u = A(\eta+\lambda)^{2\beta} + B(\eta+\lambda)^{-(1+2\beta)} \bullet \exp\left[-\tfrac{1}{4}(\eta+\lambda)^2\right]$$

where A and B are arbitrary constants. At $m > 0$ there is unique solution that tends to zero at infinity. At $m < 0$ two linear independent solutions decay at infinity and, hence, the original nonlinear problem may have two solutions at the same boundary conditions.

A similar analysis may be applied to system (5). Here the asymptotic solution should take the form

$$\begin{aligned} &u_0 = 1 + u; \qquad \varphi_0 = [\eta/(m+1)] + \lambda + \varphi \\ &\psi_0 = [1/(m+1)] + \psi \end{aligned}$$

The corresponding linear problem is written as

$$u'' + \{[\eta/(m+1)] + \lambda\}u' - 2\beta u = 0$$

$$\psi'' + \{[\eta/(m+1)] + \lambda\}\psi' + [2\psi/(m+1)] - 2[(1-m)/(1+m)]u = 0$$

The asymptotic solution of linear problem is

$$u = A\left(\frac{\eta}{m+1} + \lambda\right)^{4m} + B\left(\frac{\eta}{m+1} + \lambda\right)^{-(1+4m)} \times \exp\left\{-\left[\frac{\eta^2}{2(m+1)} + \lambda\eta\right]\right\}$$

$$\psi = C\left(\frac{\eta}{m+1} + \lambda\right)^{-2} + D\left(\frac{\eta}{m+1} + \lambda\right) \times \exp\left\{-\left[\frac{\eta^2}{2(m+1)} + \lambda\eta\right]\right\} + \frac{1-m}{1+2m}u$$

where A, B, C, and D are arbitrary constants.

Thus, at any m (including $m = 0$) there are two linear independent solutions that decay at infinity. It means that the original nonlinear problem may have two solutions at any m. In the case where $m = 0$, one solution is obvious; this is the solution with $\psi_0 = u_0$ and only this type of solution was investigated in Refs. 1–5. This may be the most interesting physical case; however, the nonuniqueness of the solution must be taken into account in numerical calculations.

Numerical Procedure

Asymptotic Boundary Conditions

The solutions of the asymptotic boundary equations (5) were found as steady-state solutions of the time-dependent problem that was written as follows:

$$\frac{\partial u_0}{\partial t} = u_0'' + \varphi_0 u_0' + \left[\frac{2m}{(m+1)}\right](1 - u_0^2)$$

$$\frac{\partial \psi_0}{\partial t} = \psi_0'' + \varphi_0\psi_0' + \gamma\left[\psi_0^2 - \frac{1}{(m+1)^2}\right] + \left[\frac{(1-m)}{(1+m)}\right](1 - u_0^2) \tag{7}$$

$$\varphi_0' + \psi_0 = [2/(m+1)]u_0$$

Here γ is auxiliary parameter that is needed to select the different solutions. To do that the integral thickness of the ψ_0 profile

$$\delta_\psi = \int_0^\infty [1 - (m+1)\psi_0]\,d\eta$$

was prescribed, and the inverse problem was solved for Eqs. (7). The parameter γ was considered as an additional variable that was found simultaneously with other quantities. At the given value of δ_ψ only one value of γ can be found, and the condition $\gamma = 1$ corresponded to the real solutions of problem (5). The required condition can be satisfied iteratively by variation of δ_ψ. (It should be noted that at $m = 0$ the coefficient at γ may reduce to zero, and in this case the right-hand side of the second relationship in Eqs. (7) must be written as $\gamma\psi_0 - u_0^2$.)

Equations (7) are analogous to the usual boundary-layer equations, and to solve them the inverse boundary-layer problem calculation procedure[9] was used.

Thus, the numerical procedure for the calculation of boundary conditions is as follows.

1) At a given value of δ_ψ the steady-state solution of Eqs. (7) is found using the second-order scheme.[9]

2) Varying the δ_ψ in range from -0.5 to 4, the approximate location of the roots $\gamma(\delta_\psi) = 1$ are found.

3) The improved values of the roots are calculated iteratively. [Here the simple method based on successive dividing the interval with root of the equation $\gamma(\delta_\psi) = 1$ was used.]

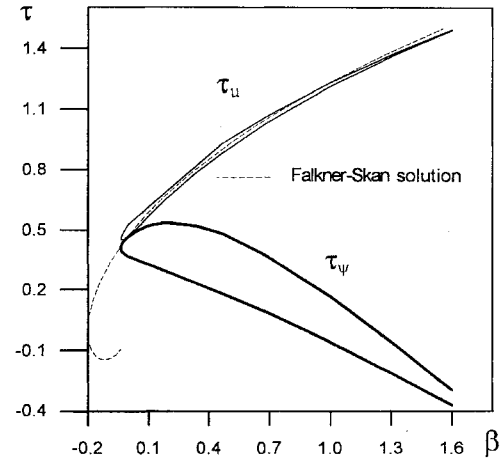

Fig. 2 Solutions of asymptotic boundary value problem.

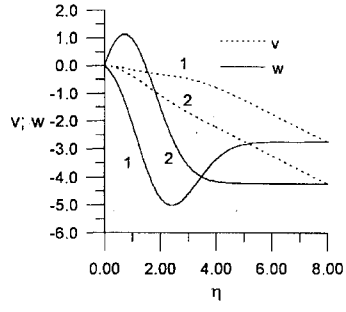

Fig. 3a Comparison of two asymptotic solutions at m = 0.5.

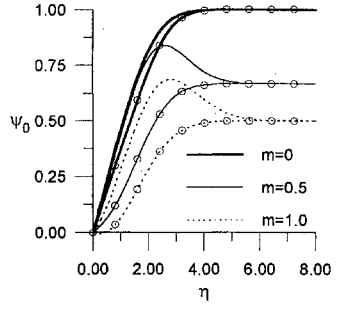

Fig. 3b Coefficients ψ_0: ——, type 1 and —⊖—, type 2.

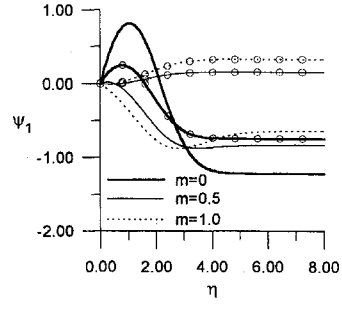

Fig. 3c Coefficients ψ_1: ——, type 1 and —⊖—, type 2.

4) The values of λ found at the preceding steps are used to obtain the numerical solutions of the linear problem (6) by the finite-difference method, the same as for the nonlinear problem.

Some results of the calculations are presented in Figs. 2 and 3. In Fig. 2 the distribution of $\tau_u = u_0'(0)$ and $\tau_\psi \equiv \psi_0'(0)$ with respect to $\beta = 2m/(m+1)$ are shown. The distribution of $\tau_u(\beta)$ for the Falkner–Skan problem is also plotted in Fig. 2 for comparison. The solution of the boundary value problem (5) exists at $m > m_{cr}$, where $m_{cr} = -0.018$, i.e., the critical value is significantly less than in the Falkner–Skan problem. There are two solutions throughout the range of m. The solution that was reduced to the Blasius solution in the case $m = 0$ will be denoted as solution 1, the other solution as solution 2. In Fig. 2 solution 1 is shown by the bottom branch of the loop and solution 2 by the top curve.

Neither distribution of $\tau_u(\beta)$ differs much from the other nor from the Falkner–Skan distribution. The difference between the u profiles is also small. The difference in cross velocities, however, is much more significant. In Fig. 3a the profiles of v and w for the two different solutions at $m = 0.5$ are compared. The profiles of v and w are calculated using the first terms of the asymptotic expansions. To obtain the w profile, it was assumed that $\zeta = 8$. The two profiles of v are rather similar to one another, but the w profiles differ even qualitatively. The different solutions correspond to the opposite directions of secondary flows inside the boundary layer. For solution 1 the secondary flow is directed to the inward corner, for solution 2 to the outward the corner.

The variation of u, v, and φ with respect to m is qualitatively similar to the behavior of these parameters in the Falkner–Skan problem. The distributions of ψ_0 and ψ_1 (i.e., the only parameters that are inherent to the considered case) are presented in Figs. 3b and 3c. Here the profiles at several m ($m = 0, 0.5, 1.0$) for both solutions 1 and 2 are shown. The variation of the profiles is rather monotonous with respect to m.

It is interesting to note that asymptotic solution and, hence, the solution of the self-similar corner layer equations exist only at negative or very small positive streamwise pressure gradients where there is no separation. These features differ significantly from the Falkner–Skan solution.

The calculations of the boundary values were performed before the numerical integration of corner layer equations, and the results were stored in computer memory.

Corner Layer Equations

When the boundary values are calculated, the numerical solution of the corner layer equations can be obtained. To find both types of solutions, the dependent variables were presented as a combination of asymptotic functions and disturbances (°):

$$u = u_0(\eta) + u^\circ, \qquad \varphi = \varphi_0(\eta) + \varphi^\circ$$
$$\psi = \psi_0(\eta)\zeta + \psi_1(\eta) + \psi^\circ, \qquad \theta = \theta_0(\eta)\zeta + \theta_1(\eta) + \theta^\circ$$

Additionally, the last two relationships in Eqs. (1) were replaced by Poisson's equations that were obtained by differentiation of the original equations. Thus, the equations suitable for numerical calculations are written as

$$\begin{aligned}
&\Delta u^\circ + \varphi u^\circ_\eta + \psi u^\circ_\zeta + \left\{\varphi^\circ u_0' - [2m/(m+1)]\left(2u_0u^\circ + u^{\circ 2}\right)\right\} = 0\\
&\Delta\theta^\circ + \varphi\theta^\circ_\eta + \psi\theta^\circ_\zeta + \left\{\varphi^\circ(\theta_0'\zeta + \theta_1') + \psi^\circ\theta_0\right.\\
&\quad + [2/(m+1)]\left[\left(u_0 + u^\circ\right)\theta^\circ + u^\circ(\theta_0\zeta + \theta_1)\right]\\
&\quad + 2[(m-1)/(m+1)]\left[\left(u_0 + u^\circ\right)\left(\zeta u^\circ_\eta - \eta u^\circ_\zeta\right)\right.\\
&\quad \left.\left. + u_0'u^\circ\zeta\right]\right\} = 0\\
&\Delta\varphi^\circ = \left[2u^\circ_\eta/(m+1)\right] - \theta^\circ_\zeta\\
&\Delta\psi^\circ = \left[2u^\circ_\zeta/(m+1)\right] + \theta^\circ_\eta
\end{aligned} \tag{8}$$

The boundary conditions for these equations reduced to

$$\begin{aligned}
&\eta = 0: u^\circ = \varphi^\circ = \psi^\circ = 0; \qquad \theta^\circ = \psi^\circ_\eta\\
&\zeta = \zeta_m: u^\circ = \varphi^\circ = \psi^\circ = \theta^\circ = 0\\
&u^\circ(\eta, \zeta) = u^\circ(\zeta, \eta) + u_0(\zeta) - u_0(\eta)\\
&\varphi^\circ(\eta, \zeta) = \psi^\circ(\zeta, \eta) + \psi_0(\zeta)\eta + \psi_1(\zeta) - \varphi_0(\eta)\\
&\psi^\circ(\eta, \zeta) = \varphi^\circ(\zeta, \eta) + \varphi_0(\zeta) - \psi_0(\eta)\zeta - \psi_1(\eta)\\
&\theta^\circ(\eta, \zeta) = -\theta^\circ(\zeta, \eta) - \theta_0(\eta)\zeta + \theta_1(\eta) + \theta_0(\zeta)\eta + \theta_1(\zeta)
\end{aligned} \tag{9}$$

The problems (8) and (9) are weakly nonlinear and all variables decay at $\zeta \to \infty$. Such formulations allow the converged numerical solution for both types of asymptotic boundary conditions to be obtained. On the other hand, for equations taken in form of Eqs. (1), numerical instability takes place, especially when the right computational boundary was located at $\zeta > 10$.

The solution of the boundary value problems (8) and (9) was found to be the steady-state solution of the time dependent problem that contained time derivatives in the right-hand side. The left-hand side was approximated by a central difference scheme, excluding the convective terms such as φu_η. Those terms were approximated by an upwind first-order scheme. Thus, taken as a whole, the finite difference scheme was a first-order scheme, and to reduce the truncation errors, a rather fine grid was used. Taking into account that the number of variants is limited, however, such an approach was a reasonable compromise between the expenses needed for development of the numerical code and the expenses needed for calculations.

The finite difference equations were solved by the overrelaxation method with a relaxation parameter equaling $\frac{3}{2}$ and a time step equaling 0.5. The solution was considered steady state if the maximum difference between the parameters at neighboring time steps was less than 5×10^{-5}.

Results of Numerical Calculations

The calculations were performed on a uniform grid with equal steps in the ζ and η directions: $\Delta\eta = \Delta\zeta = \zeta_m/(N-1)$, where ζ_m is the location of the right computational boundary and N is the maximum number of grid nodes in one direction. The influence of the parameters ζ_m and N on the solution was studied in the case $m = 0$, type 2.

In Figs. 4a and 4b the influence of the right computational boundary location is shown. Here ζ_m was varied but the step size was the same for all cases and equals $\Delta\zeta = 0.5$ (which means that at $\zeta_m = 10$, the N equals 21 and so on). In this figure the distributions of the velocities along the diagonal $[u(\eta = \zeta),\ v = w(\eta = \zeta)]$ are presented. It is seen that cross velocity is the most influenced by ζ_m. At $\zeta_m \geq 30$, however, even this influence become practically negligible.

In Figs. 4c and 4d the influence of nodes number is shown. The same parameters as in Figs. 4a and 4b are presented. In the case where $N = 181$ the solution is practically independent of grid step. Thus, all other calculations were performed with $\zeta_m = 30$, and $N = 181$.

In Fig. 5 the calculations for case $m = 0$, type 1 are compared with known data. The distributions of the streamwise velocity along the diagonal and the distribution of friction along the wall $[\tau_u = u_\eta(0, \zeta)]$ are compared with Rubin and Grossman's data.[3] The distribution of cross velocity along the diagonal is compared with Ghia data[4] also. Other parameters obtained by Ghia are not plotted because they are very close to Rubin and Grossman's data. The streamwise velocity profile and friction distribution agree with known data rather well. The agreement of the cross velocities profile with Rubin and Grossman's data is rather poor and can be explained by the use of a coarse grid in their calculations ($\zeta_m = 8.8$, $N = 12$). Moreover, they could not shift the right computational boundary farther mentioned location, because of the numerical instability taking place. The agreement with Ghia data obtained on a finer grid is good. Some discrepancy is observed only at large η; however, the asymptotic values of cross velocity are practically identical in both cases: $V(\infty) = 1.2$.

The influence of streamwise pressure gradients on flow structure and comparison of the two types of solutions are shown in Figs. 6–8. In Fig. 6 the longitudinal velocity contours are plotted. Here only the type 1 solution is presented, because the different types of streamwise velocity distribution are qualitatively similar. In accelerated flow, the longitudinal velocity profiles are fuller and the corner layer thickness is thinner. Near the corner the velocity increases more rapidly than far from the corner. The streamwise flow structures are qualitatively similar at all $m > 0$, as are they for the Falkner–Skan solution. At small negative $m \geq m_{cr}$ the flow structure is close to the case $m = 0$.

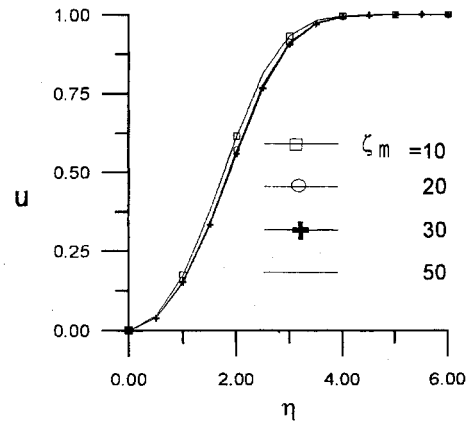

a)

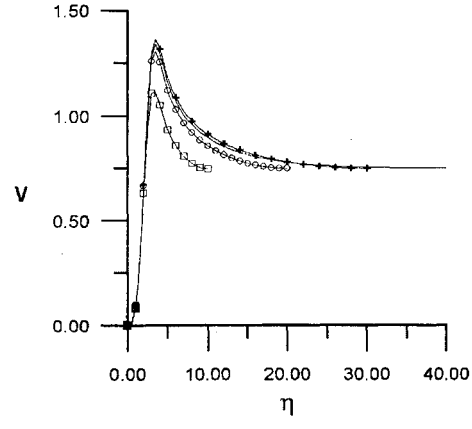

b)

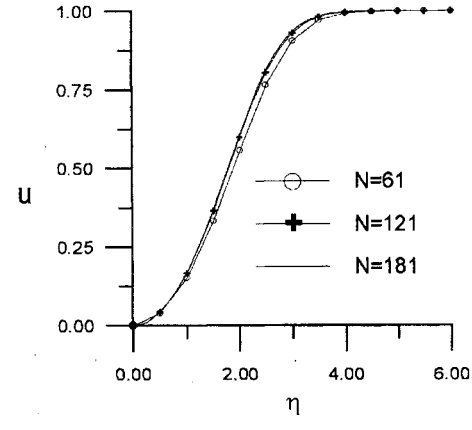

c)

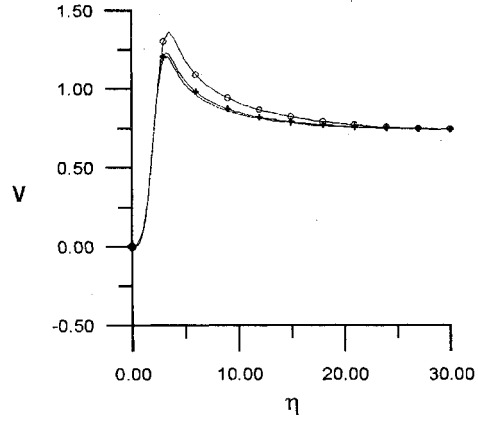

d)

Fig. 4 Influence of computational boundary location and number of grid nodes on the velocities on diagonal; $m = 0$, type 2.

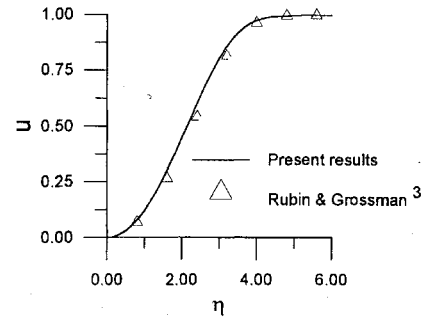

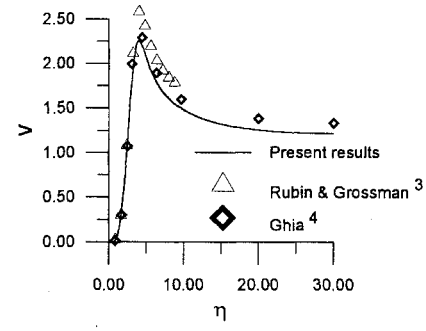

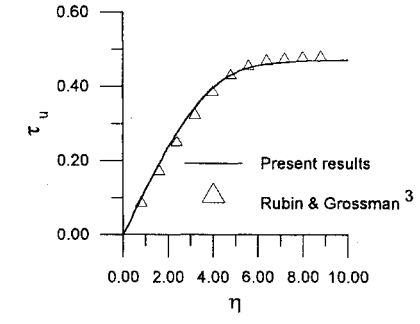

Fig. 5 Comparison of present results with known data; $m = 0$, type 1.

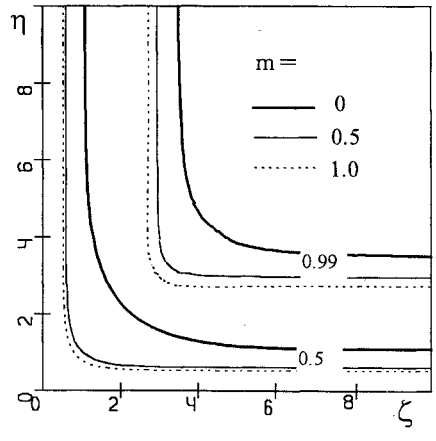

Fig. 6 Streamwise velocity contours.

The patterns of secondary flow structures for three cases ($m = 0, 0.5, 1$) are plotted in Fig. 7. At $m = 0$, the secondary flow outside the boundary layers is directed outward to the corner. For type 2 solution this picture remains the same inside boundary layers also, but in type 1 solution there are regions of inward flows near the walls. At $m = 0.5$, the main secondary flow is directed to the inward corner, but the solutions of type 1 and 2 change their roles (i.e., in type 2 solution there are regions of outward flows near the walls, but in type 1 solution there are not). At larger m ($m \geq 1$), the qualitative difference between the two solutions disappears, and the secondary flow is directed to every inward corner. Here, the most characteristic regimes are presented. At intermediate

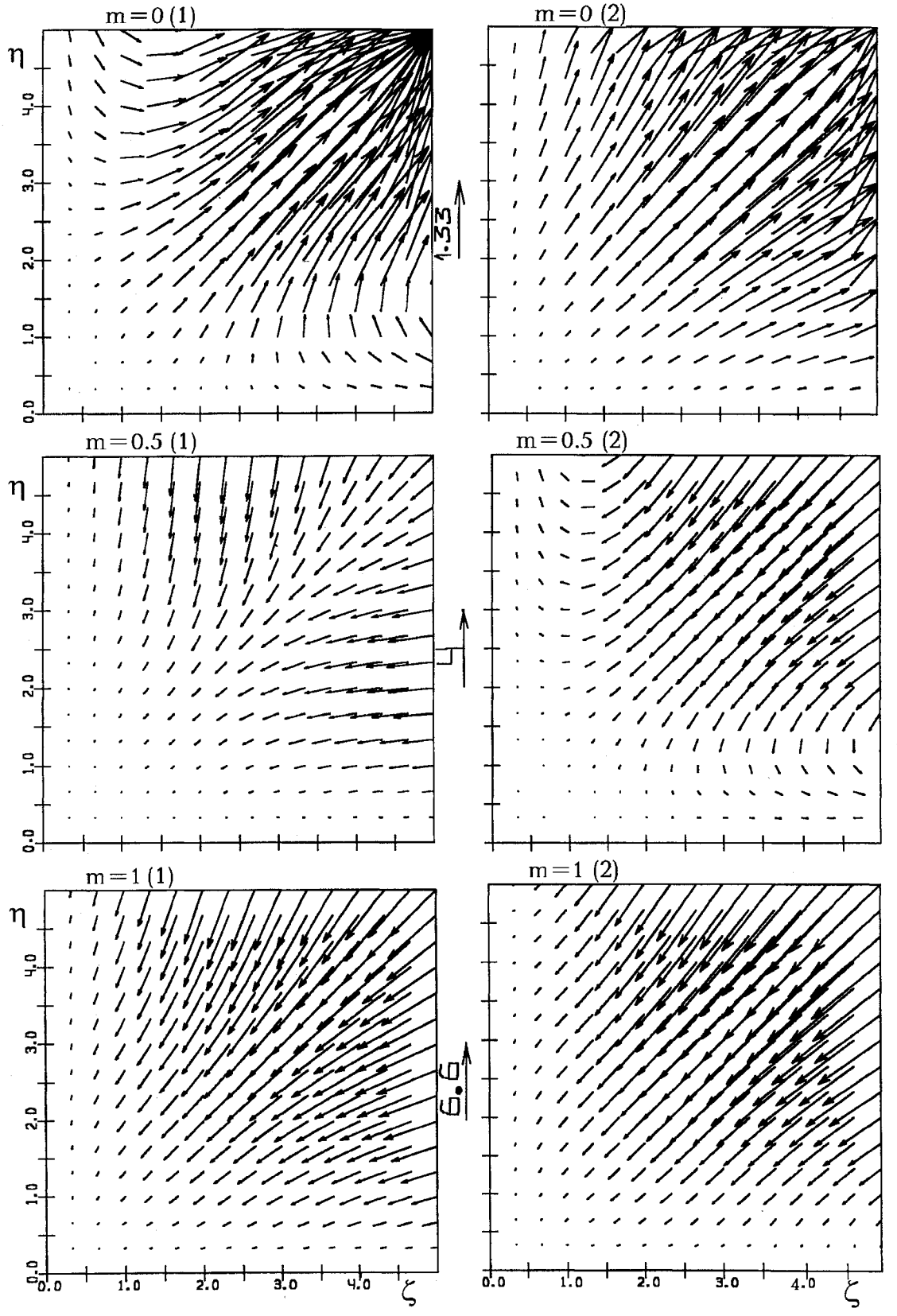

Fig. 7 Secondary flow patterns.

values of m, the smooth variation from one typical regime to another takes place. At the critical value of $m = m_{cr}$, the secondary flow structure is qualitatively similar to structure in case $m = 0$, type 2.

In Fig. 8 the streamwise vorticity contours are presented. The normalized value of the streamwise vorticity is determined as: $\Omega = w_\eta - v_\zeta = (1-m)(\zeta u_\eta - \eta u_\zeta) - (m+1)$. The real vorticity ω is connected to Ω by the relationship $\omega = (U_e/2x)\Omega$. On each side, from the diagonal, there are two regions of vorticity with vortices of opposite signs. These regions are not closed but are stretched along the walls. Below the diagonal, the upper vortex has a positive sign in the type 1 solution and a negative sign in the type 2 solution. Qualitatively the distributions of vorticity are similar at all m (for definite type of solution) and the differences are only quantitative.

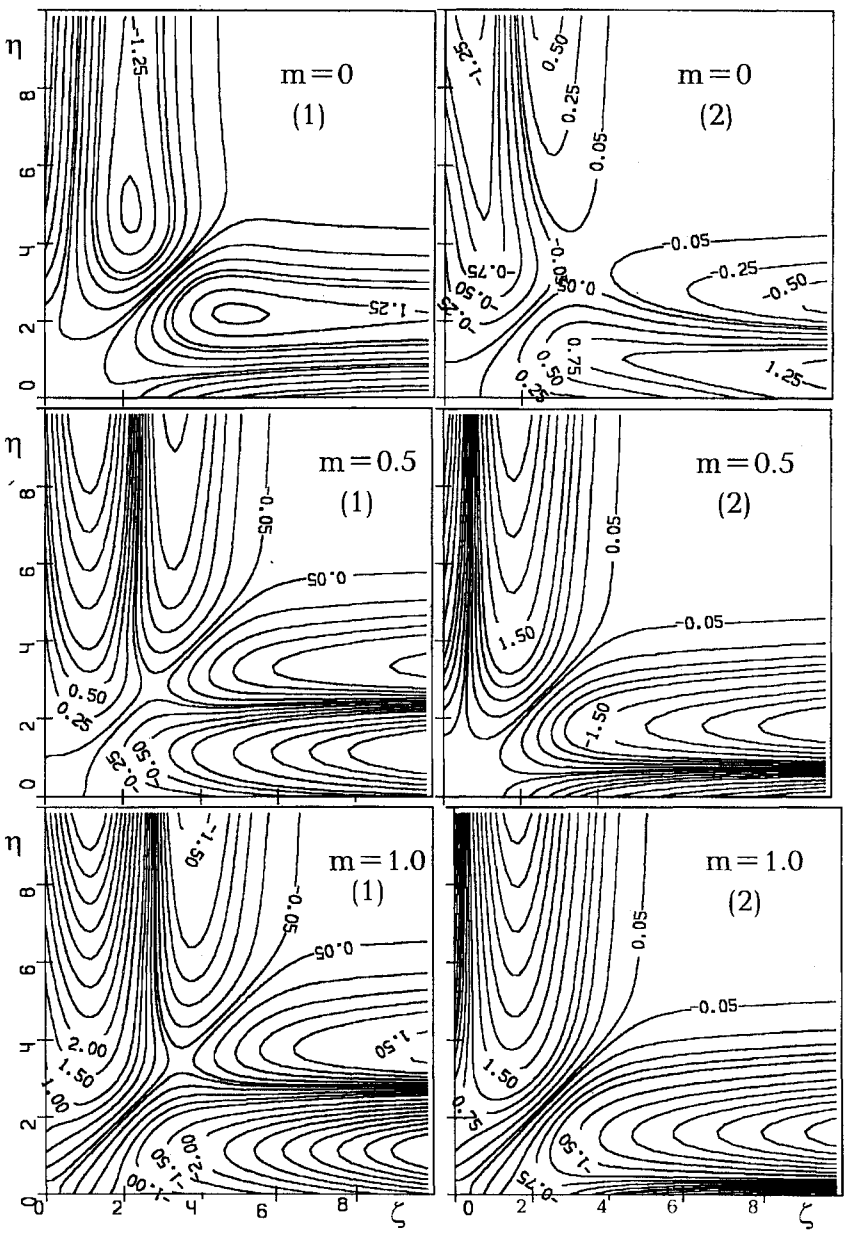

Fig. 8 Streamwise vorticity contours.

Conclusions

1) The corner layer equations describing the self-similar incompressible flow along a right-angle unbounded corner with a nonzero streamwise pressure gradient are derived. The method of numerical integration of these equations is developed.

2) It is shown that the equations have two solutions at $m \geq m_{cr} = -0.018$.

3) The numerical solutions of the corner layer equations at several m in the range $1 \geq m \geq m_{cr}$ are obtained.

References

[1]Rubin, S. G., "Incompressible Flow Along a Corner," *Journal of Fluid Mechanics*, Vol. 26, Sept. 1966, pp. 97–110.

[2]Pal, A., and Rubin, S. G., "Asymptotic Features of Viscous Flow Along a Corner," *Quarterly of Applied Mathematics*, Vol. 29, April 1971, pp. 91–108.

[3]Rubin, S. G., and Grossman, B., "Viscous Flow Along a Corner: Numerical Solution of the Corner Layer Equations," *Quarterly of Applied Mathematics*, Vol. 29, July 1971, pp. 169–186.

[4]Ghia, K. N., "Streamwise Flow Along an Unbounded Corner," *AIAA Journal*, Vol. 13, No. 7, 1975, pp. 902–907.

[5]Michail, A. G., and Ghia, K. N., "Viscous Compressible Flow in the Boundary Region of an Axial Corner," *AIAA Journal*, Vol. 16, No. 9, 1978, pp. 931–939.

[6]Patankar, S. V., and Spalding, D. B., "A Calculation Procedure for Heat, Mass and Momentum Transfer in Three-Dimensional Parabolic Flows," *International Journal of Heat and Mass Transfer*, Vol. 15, No. 10, 1972, pp. 1787–1806.

[7]Schlichting, H., *Boundary Layer Theory*, McGraw–Hill, New York, 1979, p. 817.

[8]Olver, F. W. J., *Introduction to Asymptotic and Special Functions*, Academic, New York, 1974, p. 403.

[9]Vasiliev, V. I., "Computation of Separated Duct Flows Using Boundary-Layer Equations," *AIAA Journal*, Vol. 32, No. 6, 1994, pp. 1191–1199.